Work published on Signal Processing 117 pp. 115-125, 2015, DOI 10.1016/j.sigpro.2015.05.005

Frequency Estimation by Two- or Three-Point Interpolated Fourier Algorithms based on Cosine Windows

Daniel Belega[1] and Dario Petri[2]

[1] Department of Measurements and Optical Electronics, "Politehnica" University of Timişoara,

Bv. V. Pârvan, Nr. 2, 300223, Timişoara, Romania,

Phone: +40 2 56 40 33 65, Fax : +40 2 56 40 33 62, E-mail: *daniel.belega@upt.ro*

[2] Department of Electrical Engineering, University of Trento,

Trento 38123, Italy,

Phone: +39 0461 883902, Fax: +39 0461 882093, E-mail: *dario.petri@unitn.it*

Abstract *— This paper investigates the frequency estimation of a complex sinusoid obtained by interpolating two or three samples of the Discrete-Time Fourier Transform (DTFT) of a signal weighted by a suitable cosine window. Versions of the algorithms based on both DTFT complex values or modules are considered and the expressions for the related frequency estimators are provided. Iterative procedures are used in order to minimize the estimator variance due to additive wideband noise. Furthermore, the accuracies of the proposed estimators are verified and compared each other and with state-of-the art algorithms by means of computer simulations when applied to noisy or noisy and harmonically distorted complex sinusoids, respectively.*

Index-Terms: Frequency estimation, Fourier interpolation, complex sinusoids, statistical analysis, windowing.

1. Introduction

Real-time frequency estimation of a sinusoid is often required in many engineering applications such as communications, audio systems, radar, sonar, power systems, measurement and instrumentation. It is well-know that the peak location of the Discrete Time Fourier Transform (DTFT) of the overall signal represents the maximum likelihood frequency estimate of a sinusoid embedded in additive wideband Gaussian noise [1]. Such a peak can be effectively and accurately located using a two-step search procedure. In the first step (called coarse-search) the frequency bin corresponding to the Discrete Fourier Transform (DFT) sample of largest magnitude is determined through a simple maximum search routine. In the second step (called fine-search) an accurate estimate of the interbin frequency location is obtained. The sum of the two procedure outputs then provides the desired frequency estimate. Various methods have been proposed in the scientific literature for fine-search implementation of either complex sinusoids [2-11] or real sinusoids [1, 12-20] by interpolating two or more DFT complex samples or modules. In particular, more than two DFT samples are used when estimating the frequency of a real sinusoid in order to reduce the effect of the spectral interference from the image component [17-20], but at the cost of an increased wideband noise sensitivity of the related frequency estimator [19]. Also, more DFT samples are used in [11] to reduce the gap between the performance of the estimator proposed in [6] and the related unbiased Cramer-Rao Lower Bound (CRLB).

Two- or three-point interpolated Fourier algorithms are often used when estimating the frequency of a complex sinusoid [2-10]. The effect of wideband noise on the estimates returned by two interpolation points algorithms is minimized when using the Aboutanios and Mulgrew (AM) algorithm [8]. That algorithm requires two DTFT samples located exactly halfway between adjacent DFT samples and it returns a frequency estimator with a variance very close to the related unbiased CRLB by using an iterative procedure. However, only two iterations suffice to reach asymptotic accuracy [8]. Two different but equally accurate versions of the AM algorithm are proposed, based on DTFT complex values or modules, respectively. Conversely, a bias-corrected three-point interpolated Fourier algorithm relying only on complex DFT samples has been proposed by Candan in [5], specifically designed for signal records

with a small number of samples. It approaches the Jacobsen estimator [4] when the number of analyzed samples is quite high, as occurs in many engineering applications. Both the AM and the Jacobsen algorithms are based on the rectangular window since only complex sinusoids are considered and the effect on the returned estimator of the interference due to spectral leakage from other possible signal tones is assumed to be negligible with respect to the effect of wideband noise. However, signals affected by disturbance tones are often encountered in practical applications so techniques to reduce their detrimental effect on frequency estimates need to be applied. Very recently, a bias-corrected iterative three-point interpolated Fourier procedure based on windowed data has been proposed in [10]. It returns accurate estimates even when only few data samples are analyzed, while requiring a smaller processing effort than the procedure proposed in [16].

The aim of this paper is to generalize both AM and Jacobsen algorithms to the case when the acquired signal is multiplied by a generic cosine window [21], in order to reduce the effect of spectral leakage from interfering tones on the estimated frequency. In addition, the module based version of the three-point interpolated Fourier algorithm is introduced and the iterative procedure proposed in [8], [10], or [11] to minimize the estimator variance due to wideband noise is applied to both versions of the three-point interpolated Fourier algorithm.

Two different versions of two- or three-point weighted interpolated Fourier algorithms minimizing the estimator variances (simply called MV-IpDTFT(2) and MV-IpDTFT(3), respectively) are proposed. It is worth noticing that the AM algorithm is the particular case of the MV-IpDTFT(2) algorithm based on the rectangular window, while the Jacobsen algorithm corresponds to the MV-IpDTFT(3) version 1 based on the rectangular window. The expressions of the proposed estimators and the related variances due to wideband noise are derived. Furthermore, the accuracies of the derived estimators are compared each other through computer simulations in the case of noisy or noisy and harmonically distorted complex sinusoids, respectively.

The remaining of the paper is organized as follows. In Section 2 the expressions of the estimators provided by the MV-IpDTFT(2) and MV-IpDTFT(3) algorithms related to the first iteration are derived.

In addition, the steps required by the procedures related to the proposed algorithms are described. The expressions for the variances of the proposed estimators and the constraints under which windowing is advantageous are then derived in Section 3. The accuracies of the derived expressions for the estimator variances are verified through computer simulations in Section 4. Moreover, in this section the accuracies of the considered estimators are then analyzed and compared each other by means of computer simulations in the case of noisy or noisy and harmonically distorted complex sinusoids. Finally, Section 5 concludes the paper.

2. The proposed two- or three-point Fourier estimators

The analyzed signal is modelled as:

$$x(m) = Ae^{j(2\pi fm+\phi)} + e(m), \qquad m = 0,1,2,\ldots,M-1 \tag{1}$$

where A, f, and ϕ are respectively the amplitude, the frequency, and the phase of the complex sinusoid, $e(\cdot)$ is a complex additive white Gaussian noise of zero mean and variance σ^2, and M is the number of acquired samples. The frequency f can be expressed as:

$$f = \frac{f_{in}}{f_s} = \frac{\nu}{M} = \frac{l+\delta}{M}, \tag{2}$$

where f_{in} is the frequency of the continuous-time complex sinusoid, f_s is the sampling frequency, ν represents the number of acquired sinusoid cycles, l is its rounded value and δ ($-0.5 \le \delta < 0.5$) is the differences between ν and l. Coherent sampling implies $\delta = 0$, but usually non-coherent sampling occurs in practice [22].

The analyzed signal (1) is weighted by a suitable window function $w(\cdot)$, so obtaining the signal: $x_w(m) = x(m)\cdot w(m)$, $m = 0, 1,\ldots, M-1$. Windows belonging to the cosine-class are usually employed [13, 20]:

$$w(m) = \sum_{h=0}^{H-1} a_h \cos\left(2\pi \frac{h}{M} m\right), \quad m = 0,1,\ldots,M-1 \tag{3}$$

where $H \geq 1$ represents the number of window coefficients a_h, $h = 0, \ldots, H - 1$. This class of windows will be used in the remaining of the paper.

The DTFT of the windowed signal $x_w(\cdot)$ is given by:

$$X_w(\lambda) = AW(\lambda - \nu)e^{j\phi} + E_w, \tag{4}$$

where $W(\cdot)$ is the DTFT of the adopted window, and $E_w(\cdot)$ is the DTFT of weighted wideband noise.

We assume that the wideband noise power is negligible as compared with the complex sinusoid one. Hence, the DTFT of the windowed signal can be expressed as:

$$X_w(\lambda) \cong AW(\lambda - \nu)e^{j\phi}. \tag{5}$$

Assuming that the number of acquired samples is high enough ($M >> 1$), after some algebraic calculations, the expression of the DTFT of the window $w(\cdot)$ can be written as:

$$W(\lambda) = \frac{M \sin(\pi\lambda)}{\pi} \sum_{h=0}^{H-1} (-1)^h a_h \frac{\lambda}{\lambda^2 - h^2} e^{-j\pi\lambda} = \tilde{W}(\lambda) e^{-j\pi\lambda}, \tag{6}$$

where

$$\tilde{W}(\lambda) \stackrel{\Delta}{=} \frac{M \sin(\pi\lambda)}{\pi} \sum_{h=0}^{H-1} (-1)^h a_h \frac{\lambda}{\lambda^2 - h^2}. \tag{7}$$

Using (7), after some algebra, the following expression for the derivative of $\tilde{W}(\cdot)$ is achieved:

$$\tilde{W}'(\lambda) = \frac{M}{\pi} (\sin(\pi\lambda) + \pi\lambda \cos(\pi\lambda)) \sum_{h=0}^{H-1} (-1)^h a_h \frac{1}{\lambda^2 - h^2} - \frac{2M}{\pi} \lambda^2 \sin(\pi\lambda) \sum_{h=0}^{H-1} (-1)^h a_h \frac{1}{(\lambda^2 - h^2)^2}. \tag{8}$$

Expressions (7) and (8) show that $\tilde{W}(\cdot)$ is a even function, while its derivative $\tilde{W}'(\cdot)$ is an odd function.

It is also worth noticing that the H-term Maximum Sidelobe Decay (MSD) window ($H \geq 2$), known also as the Rife-Vincent class I windows [1], belonging to the cosine class windows, are frequently used in the scientific literature. Indeed they exhibit the highest sidelobe decay rate (equal to $6(2H - 1)$ dB/octave) for a given number H of window terms [21], so providing the highest rejection capability of interference from distant spectral tones, which is a situation that occurs when the number of acquired sine-wave cycles

is not too small. In particular, the two-term MSD window, known also as the Hann window, is frequently employed in practice. The coefficients of the *H*-term MSD window ($H \geq 2$) can be expressed as $a_0 = C_{2H-2}^{H-1} / 2^{2H-2}$, $a_h = C_{2H-2}^{H-h-1} / 2^{2H-3}$, $h = 1, 2, \ldots, H-1$ and the related DTFT reduces to [14]:

$$W(\lambda) = \frac{M \sin(\pi\lambda)}{2^{2H-2}\pi\lambda} \frac{(2H-2)!}{\prod_{h=1}^{H-1}(h^2-\lambda^2)} e^{-j\pi\lambda}, \quad \text{for } |\lambda| << M \tag{9}$$

A. ***The frequency estimators provided by the two-point algorithms***

The expressions used for estimating the sine-wave frequency in each single step of the procedure based on two DTFT interpolation points (either complex values or modules) are provided by the following theorem.

Theorem 1: *The estimators* $\hat{\delta}_{2p}^{(c)}$ and $\hat{\delta}_{2p}^{(m)}$ *for the normalized fractional frequency* δ *are:*

$$\hat{\delta}_{2p}^{(c)} = \gamma_{2p} \operatorname{Re}\left\{ \frac{X_w(l+0.5) + X_w(l-0.5)}{X_w(l+0.5) - X_w(l-0.5)} \right\}, \tag{10}$$

and

$$\hat{\delta}_{2p}^{(m)} = \gamma_{2p} \frac{|X_w(l+0.5)| - |X_w(l-0.5)|}{|X_w(l-0.5)| + |X_w(l+0.5)|}. \tag{11}$$

where $\gamma_{2p} = \dfrac{\sum_{h=0}^{H-1} (-1)^h a_h \dfrac{1}{1-4h^2}}{2\sum_{h=0}^{H-1} (-1)^h a_h \dfrac{1+4h^2}{(1-4h^2)^2}}$.

The proof of that theorem is given in Appendix A. In particular, when *H*-term MSD windows are adopted, (A.5) and (A.8) in the Appendix A return $\gamma_{2p} = H - 0.5$. Also, when the rectangular window is used (i.e. $H = 1$), we have $\gamma_{2p} = 0.5$.

The iterative procedures that implement the MV-IpDTFT(2) algorithm are specified in Table 1, where the estimators (10) or (11) are used, according to the chosen version of the algorithm.

Table 1. The iterative procedures implementing the MV-IpDTFT(2) estimators.

Step 1: i: = 0 and $\hat{\delta}_{2p(0)} = 0$

Step 2: i := i + 1

Step 3: $X_w\left(l+\hat{\delta}_{2p(i-1)}+p\right)=\sum_{m=0}^{M-1} x_w(m)e^{-j2\pi\frac{l+\hat{\delta}_{2p(i-1)}+p}{M}m}, \quad p=\pm 0.5$

$\hat{\delta}_{2p(i)} = \hat{\delta}_{2p(i-1)} + h_{2p}\left(\hat{\delta}_{2p(i-1)}\right)$, *where*

$$h_{2p}\left(\hat{\delta}_{2p(i-1)}\right)=\gamma_{2p}\,\mathrm{Re}\left\{\frac{X_w(l+\hat{\delta}_{2p(i-1)}+0.5)+X_w(l+\hat{\delta}_{2p(i-1)}-0.5)}{X_w(l+\hat{\delta}_{2p(i-1)}+0.5)-X_w(l+\hat{\delta}_{2p(i-1)}-0.5)}\right\}, \qquad \textit{version 1}$$

$$h_{2p}\left(\hat{\delta}_{2p(i-1)}\right)=\gamma_{2p}\,\frac{\left|X_w(l+\hat{\delta}_{2p(i-1)}+0.5)\right|-\left|X_w(l+\hat{\delta}_{2p(i-1)}-0.5)\right|}{\left|X_w(l+\hat{\delta}_{2p(i-1)}-0.5)\right|+\left|X_w(l+\hat{\delta}_{2p(i-1)}+0.5)\right|}, \qquad \textit{version 2}$$

in which $\gamma_{2p}=\dfrac{\sum_{h=0}^{H-1}(-1)^h a_h \dfrac{1}{1-4h^2}}{2\sum_{h=0}^{H-1}(-1)^h a_h \dfrac{1+4h^2}{\left(1-4h^2\right)^2}}$

Step 4: repeat Steps 2 and 3 once.

It is worth noticing that when the rectangular window is used the above procedure reduces to the AM algorithm [8].

B. ***The frequency estimators provided by the three-point algorithms***

The expressions used for estimating the sine-wave frequency in each single step of the procedure based on three DTFT interpolation points (either complex values or spectral samples) are provided by the following theorem.

Theorem 2: *The estimators* $\hat{\delta}_{3p}^{(c)}$ and $\hat{\delta}_{3p}^{(m)}$ *for the normalized fractional frequency* δ *are:*

$$\hat{\delta}_{3p}^{(c)} = \gamma_{3p}\,\mathrm{Re}\left\{\frac{X_w(l+1)-X_w(l-1)}{X_w(l-1)-2X_w(l)+X_w(l+1)}\right\}, \tag{12}$$

and

$$\hat{\delta}_{3p}^{(m)} = \gamma_{3p}\,\frac{|X_w(l+1)|-|X_w(l-1)|}{|X_w(l-1)|+2|X_w(l)|+|X_w(l+1)|}, \tag{13}$$

where $\gamma_{3p} = \dfrac{a_0 + 0.5a_1}{a_0 - \dfrac{a_1}{4} - \displaystyle\sum_{h=2}^{H-1}(-1)^h \frac{a_h}{h^2-1}}$.

The proof of that theorem is given in Appendix B.

When the *H*-term MSD window is adopted we have $\gamma_{3p} = H$. It is worth noticing that the estimator (13) has been already achieved in [17] when the rectangular or the Hann window is applied to real sinusoids and in [18] when a generic window is employed. Also, in the particular case of rectangular window (H = 1 and γ_{3p} = 1), expression (12) coincides with the Jacobsen estimator [4].

It is worth noticing that the estimator $\hat{\delta}_{3p}^{(m)}$ is not provided by (13) when the rectangular window is used since different signs associate to the DFT spectrum samples $|X_w(l-1)|$ and $|X_w(l+1)|$ because one of them falls outside the window spectrum main lobe [17], [19]. Therefore, this particular case will not be considered in the following.

The iterative procedures that implement the MV-IpDTFT(3) algorithm are specified in Table 2, where the estimators (12) or (13) are used, according to the chosen version of the algorithm.

Table 2. The iterative procedures implementing the MV-IpDTFT(3) estimators.

Step 1: i: = 0 and $\hat{\delta}_{3p(0)} = 0$

Step 2: i := i + 1

Step 3: $X_w\left(l+\hat{\delta}_{3p(i-1)}+p\right)=\sum_{m=0}^{M-1} x_w(m) e^{-j2\pi\frac{l+\hat{\delta}_{3p(i-1)}+p}{M}m}, \quad p=-1,0,1$

$\hat{\delta}_{3p(i)} = \hat{\delta}_{3p(i-1)} + h_{3p}\left(\hat{\delta}_{3p(i-1)}\right)$, *where*

$$h_{3p}\left(\hat{\delta}_{3p(i-1)}\right)=\gamma_{3p}\,\mathrm{Re}\left\{\frac{X_w(l+\hat{\delta}_{3p(i-1)}+1)-X_w(l+\hat{\delta}_{3p(i-1)}-1)}{X_w(l+\hat{\delta}_{3p(i-1)}-1)-2X_w(l+\hat{\delta}_{3p(i-1)})+X_w(l+\hat{\delta}_{3p(i-1)}+1)}\right\},\quad \textit{version 1}$$

$$h_{3p}\left(\hat{\delta}_{3p(i-1)}\right)=\gamma_{3p}\,\frac{\left|X_w(l+\hat{\delta}_{3p(i-1)}+1)\right|-\left|X_w(l+\hat{\delta}_{3p(i-1)}-1)\right|}{\left|X_w(l+\hat{\delta}_{3p(i-1)}-1)\right|+2\left|X_w(l+\hat{\delta}_{3p(i-1)})\right|+\left|X_w(l+\hat{\delta}_{3p(i-1)}+1)\right|},\quad \textit{version 2}$$

in which $\gamma_{3p}=\dfrac{a_0+0.5a_1}{a_0-\dfrac{a_1}{4}-\sum_{h=2}^{H-1}(-1)^h\dfrac{a_h}{h^2-1}}$.

Step 4: repeat Steps 2 and 3 once.

3. Variances of the two- and three-point interpolation estimators

In the following the expressions of the variances due to additive wide-band noise on the estimates returned by the algorithms defined in the previous Section are derived.

A. *Expressions for the variances for the two-point estimators*

The following theorem holds:

Theorem 3: *The variances of the estimators* $\hat{\delta}_{2p}^{(c)}$ and $\hat{\delta}_{2p}^{(m)}$ *are:*

$$\sigma^2_{\hat{\delta}_{2p}^{(c)}} \cong \sigma^2_{\hat{\delta}_{2p}^{(m)}} \cong \frac{\gamma_{2p}^2(1-\rho_1)+\delta^2(1+\rho_1)}{\left[\tilde{W}(-\delta+0.5)+\tilde{W}(-\delta-0.5)\right]^2}\frac{M\cdot NNPG}{SNR}. \tag{14}$$

where $SNR = A^2/\sigma^2$, *NNPG is the window Normalized Noise Power Gain [23] (see (C.9)) and* ρ_1 *is the correlation coefficient between two DTFT spectral samples located one bin apart (see (C.11)).*

The proof of that theorem is given in the Appendix C.

In particular when the rectangular window is used, we have $\gamma_{2p} = 0.5$ and $\tilde{W}(\lambda) = \frac{M \sin(\pi\lambda)}{\pi\lambda}$, so the (14) coincides with the expression derived in [8].

Since the correlation coefficient ρ_1 is positive and smaller than 1, (14) shows that the minimum variance is achieved when $\delta = 0$, i.e., when coherent sampling occurs. The iterative procedure described in Table 1 allows us to achieve that minimum value even when δ is not null [8]. In particular, simulations showed that two iterations are enough to reach an estimator variance very close to the asymptotic value [8]. Indeed, the variance of the estimator corresponding to the second iteration is very close to the value returned by (14) when $\delta = 0$ [8], i.e.,

$$\sigma^2_{\hat{\delta}_{2p(2)}} \cong \sigma^2_{\hat{\delta}_{2p(1)}}\Big|_{\delta=0} \cong \frac{\gamma^2_{2p}(1-\rho_1)}{4\left|W(-0.5)\right|^2}\frac{M \cdot NNPG}{SNR} = \frac{\gamma^2_{2p}(1-\rho_1)}{4M}\frac{ENBW}{SL^2(-0.5)}\frac{1}{SNR}. \tag{15}$$

in which *ENBW* and $SL(\delta)$ are defined as [23]:

$$ENBW \overset{\Delta}{=} \frac{NNPG}{(NPSG)^2} = 1 + 0.5\sum_{h=1}^{H-1}\left(\frac{a_h}{a_0}\right)^2, \tag{16}$$

and

$$SL(\delta) \overset{\Delta}{=} \frac{|W(\delta)|}{|W(0)|} = \frac{|W(\delta)|}{Ma_0}, \tag{17}$$

where $NPSG = a_0$ is the window Noise Power Signal Gain [14].

Since the CRLB for unbiased frequency estimator is [8]:

$$(\sigma^2_{\hat{\delta}})_{CR} \cong \frac{3}{2\pi^2 M \cdot SNR}. \tag{18}$$

from (15) it follows that the statistical efficiency of the estimator $\hat{\delta}_{2p(2)}$ can be expressed as:

$$R_{2p} = \frac{(\sigma^2_{\hat{\delta}})_{CR}}{\sigma^2_{\hat{\delta}_{2p(2)}}} \cong \frac{6}{\gamma^2_{2p}(1-\rho_1)\pi^2}\frac{SL^2(-0.5)}{ENBW}. \tag{19}$$

Thus, the statistically efficiency increases when $SL(-0.5)$ increases and *ENBW* decreases, which occurs when the number of the window coefficients *H* decreases. Thus, the highest efficiency is achieved when

the rectangular window is adopted, for which $\gamma_{2p} = 0.5$, $\rho_1 = 0$, $SL(-0.5) = 2/\pi$, and $ENBW = 1$, and it is equal to $R_{2p} \cong 96/\pi^4 \cong 0.9855$ [8].

B. ***Expressions for the variances of the three-point estimators***

The following theorem holds:

Theorem 4: *The variances of the estimators* $\hat{\delta}_{3p}^{(c)}$ and $\hat{\delta}_{3p}^{(m)}$ *are:*

$$\sigma^2_{\hat{\delta}_{3p}^{(c)}} \cong \sigma^2_{\hat{\delta}_{3p}^{(m)}} \cong \frac{\gamma_{3p}^2(1-\rho_2) + \delta^2(3+4\rho_1+\rho_2)}{\left[\widetilde{W}(-\delta-1) + 2\widetilde{W}(-\delta) + \widetilde{W}(-\delta+1)\right]^2} \frac{M \cdot NNPG}{SNR}. \tag{20}$$

where, in addition to the parameters already defined, ρ_2 *is the correlation coefficient between two DTFT spectral samples located two bins apart (see (D.10)).*

The proof of that theorem is given in the Appendix D.

Since the correlation coefficients ρ_1 and ρ_2 are positive and smaller than 1, (20) shows that the minimum variance is achieved when $\delta = 0$. However, as for the MV-IpDTFT(2) estimators, two iterations of the procedure described in Table 2 allows us to reach that minimum value even when δ is not null. Using (B.5)-(B.7) and (16), from (20) we can obtain:

$$\sigma^2_{\hat{\delta}_{3p(2)}} \cong \sigma^2_{\hat{\delta}_{3p(1)}}\Big|_{\delta=0} \cong \frac{\gamma_{3p}^2(1-\rho_2)}{4\left(1+\frac{a_1}{2a_0}\right)^2} \frac{ENBW}{M \cdot SNR}. \tag{21}$$

It is interesting to observe that (21) does not depend on the correlation coefficient ρ_1. Also, from (18) it follows that the statistical efficiency of (21) is:

$$R_{3p} = \frac{(\sigma^2_{\hat{\delta}})_{CR}}{\sigma^2_{\hat{\delta}_{3p(2)}}} \cong \frac{6\left(1+\frac{a_1}{2a_0}\right)^2}{\gamma_{3p}^2(1-\rho_2)\pi^2} \frac{1}{ENBW}. \tag{22}$$

Even in this case the highest efficiency is achieved when the rectangular window is adopted (i.e. $a_0 = 1$, $a_1 = 0$, $\gamma_{3p} = 1$, $\rho_2 = 0$, and $ENBW = 1$) and it is equal to $R_{3p} \cong 6/\pi^2 \cong 0.6079$, which is about 1.62 times smaller than the maximum efficiency returned by the two-point interpolation.

In general, from (19) and (22), we achieve:

$$\frac{R_{2p}}{R_{3p}} = \frac{\sigma^2_{\hat{\delta}_{3p(2)}}}{\sigma^2_{\hat{\delta}_{2p(2)}}} \cong \frac{\gamma^2_{3p}(1-\rho_2)}{\gamma^2_{2p}(1-\rho_1)} \frac{SL^2(-0.5)}{\left(1+\frac{a_1}{2a_0}\right)^2}. \tag{23}$$

which shows that the ratio R_{2p}/R_{3p} is always greater than 1. For example, in the case of rectangular window we have $R_{2p}/R_{3p} = 16/\pi^2 \cong 1.6211$, while for the Hann window $R_{2p}/R_{3p} \cong 1.4232$.

It is clear that to be advantageous, data windowing must ensure that:

$$MSE(\hat{\delta})_{rect(k)} > MSE(\hat{\delta})_{wind(k)}, \tag{24}$$

where $MSE(\hat{\delta})_{rect(k)}$ and $MSE(\hat{\delta})_{wind(k)}$ are the Mean Square Errors of the δ estimators returned by a k-point ($k = 2, 3$) interpolation algorithm when the rectangular or a cosine window ($H \geq 2$) are adopted, respectively. They are due to the effect of both nearby narrow-band interfering components (which is reduced by windowing and decreases as the number of acquired signal cycles ν increases) and wideband noise (which is amplified by the use of windows) [18]. In many practical applications, a suitable number of signal cycles ν can be acquired so that windowing can reduce the contribution of narrow-band components to a negligible level. As a consequence, the use of windowing is justified when:

$$MSE(\hat{\delta})_{rect(k)} > \sigma^2_{\hat{\delta}_{kp(2)}}, \tag{25}$$

It is worth noticing that the rectangular window should be applied if (25) is not satisfied.

Moreover, observe that the right-hand member of (25) depends only on the adopted window and can be easily determined using (15) or (21), respectively for k =2 or 3. Conversely, the left-hand member can be evaluated experimentally by asynchronously sampling that analyzing signal and acquiring more data records.

4. Computer simulations

The aim of this section is to analyze and compare the accuracies of the proposed estimators by means of computer simulations in the case of noisy or noisy and harmonically distorted complex sinusoids. The adopted windows are: the rectangular window (H = 0, a_0 = 1), the two-term MSD (or Hann) window (H = 1, a_0 = 0.5 and a_1 = 0.5), the three-term Minimum Sidelobe Level and Rapid Sidelobe Decay (MSL-RSD) window (H = 2, a_0 = 0.40897, a_1 = 0.5, and a_2 = 0.09103), and the three-term MSD window (H = 2, a_0 = 0.375, a_1 = 0.5, and a_2 = 0.125) [21]. It is worth noticing that the two-term MSD and three-term MSL-RSD windows exibit the same sidelobe decay rate, equal to 18 dB/octave, while the three-term MSD has a sidelobe decay rate equal to 30 dB/octave [21].

The amplitude of the analyzed signal is A = 1 and the number of analyzed samples is M = 128.

1) Pure complex sinusoid

Fig. 1 shows the bias of the two-point (Fig. 1(a)) and the three-point (Fig. 1(b)) estimators as a function of δ, respectively. In addition, Fig. 1(a) shows the bias of both the classical bias-corrected [5 – Eq. (13)] and the iterative bias-corrected algorithms. The observation interval length varies in the range (5, 5.5) cycles with a step of 1/50.

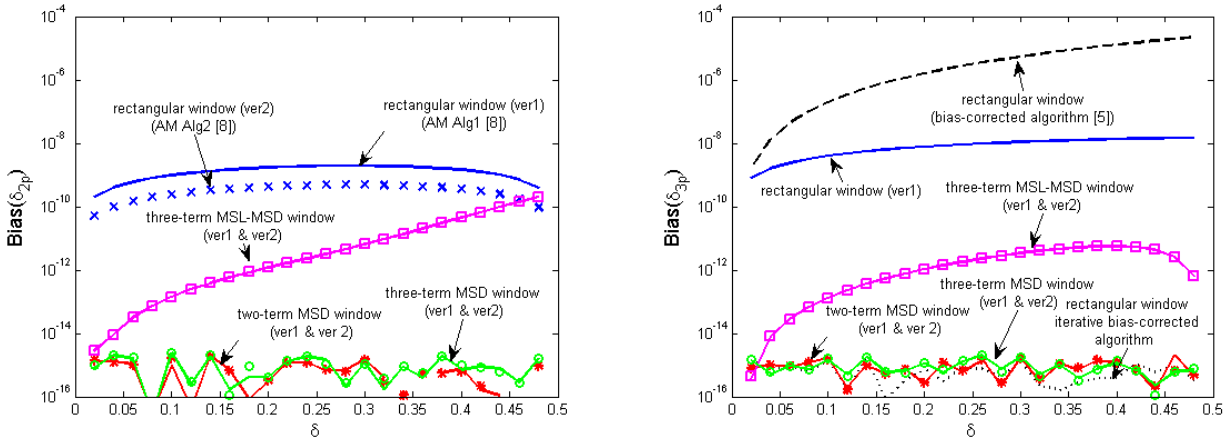

(a) (b)

Fig. 1. Bias of (a) the MV-IpDTFT(2) and (b) the MV-IpDTFT(3) estimators based on the rectangular, two-term MSD, three-term MSL-RSD, or three-term MSD windows versus δ. In (b) the bias of both the bias-corrected algorithm [5] ("dashed line") and its iterative ("dotted line") versions are also shown. The version 1 of the proposed algorithms is represented by solid lines, while the version 2 is represented by "crosses" (rectangular window), "stars" (two-term MSD window), "squares" (three-term MSL-RSD window), and "circles" (three-term MSD window). The number of analyzed sample is M = 128 and l = 5.

The values returned by simulations are always very small. However, the smallest bias is ensured by the proposed procedures when the MSD windows are adopted. Also, the values obtained in these situations are limited by rounding calculation errors. The bias related to the procedures based on the three-term MSL-RSD window is a bit higher. Moreover, with this choice the three-point algorithm outperforms the two-point one. The highest bias values are achieved when the rectangular window is adopted. In this case the algorithm version 2 (i.e. based on DTFT modules) outperforms the algorithms version 1 (i.e. based on DTFT complex values) when two-point interpolation is employed. No significant differences in the bias values related to the two algorithm versions are observed when cosine windows are adopted. Fig. 1(b) shows that the corrected-bias algorithm [5] exhibits a higher bias than the version 2 of the proposed three-point interpolation algorithm. Conversely, when the former algorithm is iterated twice the estimation bias becomes negligible.

2) Noisy complex sinusoid

Additive white Gaussian noise with zero mean and variance σ^2 corresponding to a *SNR* = 30 dB has been considered.

At first the accuracy of the expressions (14), (15) and (20), (21) for the variances $\sigma^2_{\hat{\delta}_{2p(1)}}$, $\sigma^2_{\hat{\delta}_{2p(2)}}$ and $\sigma^2_{\hat{\delta}_{3p(1)}}$, $\sigma^2_{\hat{\delta}_{3p(2)}}$, respectively, has been verified. Fig. 2 shows the statistical efficiency of the estimators provided by the two-point (Fig. 2(a)) and the three-point (Fig. 2(b)) estimators as a function of the normalized fractional frequency δ when the considered windows are adopted. The observation interval length varies in the range (4.5, 5.5) cycles with a step of 1/25. For each value of δ, 10000 runs with waveform phase ϕ uniformly distributed in the range [0, 2π) rad have been considered in computer simulations. The results returned by expressions (14), (15), and (20), (21) are also shown.

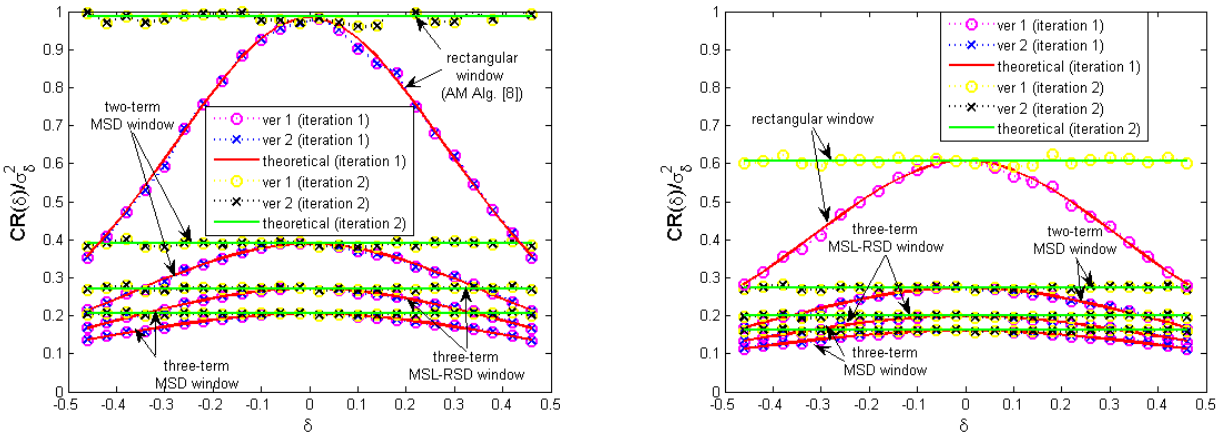

Fig. 2. Statistical efficiency of the estimators provided by (a) the MV-IpDTFT(2) and (b) the MV-IpDTFT(3) algorithms versus the normalized fractional frequency δ in the case of noisy complex sinusoid with *SNR* = 30 dB. The estimators are based on the rectangular window, two-term MSD, three-term MSL-RSD, or three-term MSD windows. The number of analyzed samples is M = 128 and l = 5. The results returned by (14), (15), and (20), (21) are also represented using solid lines.

Fig. 2 shows a very good agreement between the theoretical and the simulation results. It is worth noticing that the statistical efficiencies of the proposed estimators are almost independent of δ when two iterations are performed. Also, by comparing the curves in Fig. 2(a) and 2(b) related to a given window, it follows that the use of two-point interpolation ensures a higher statistical than the three-point interpolation [19]. Moreover, the statistical efficiency decreases as the number of window coefficients H increases.

Fig. 3 shows the MSEs of the two-point (Fig. 3(a)) and the three-point (Fig. 3(b)) estimators based on the rectangular or the two-term MSD windows, together with the CRLB for unbiased frequency estimators. The above windows have been considered since they have the highest statistical efficiencies. In the three-point estimator based on the rectangular window the version 1 is used. The MSE returned by the iterative bias-corrected approach is also reported in Fig. 3(b). The SNR varies in the range [0, 60] dB with a step of 5 dB and the number of acquired signal cycles is ν = 5.3. For each value of SNR, 10000 runs with waveform phase ϕ uniformly distributed in the range [0, 2π) rad have been considered.

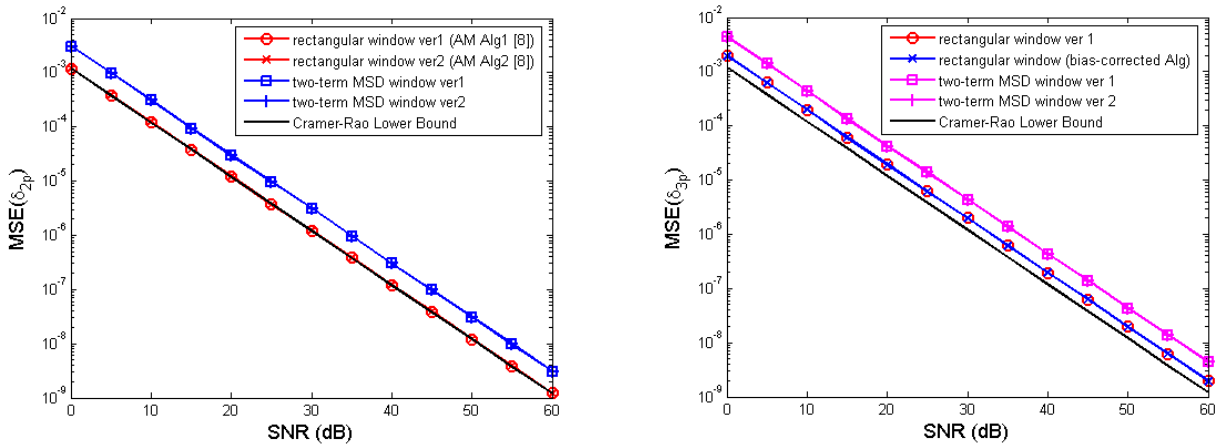

Fig. 3. MSEs values returned by (a) the MV-IpDTFT(2) and (b) the MV-IpDTFT(3) estimators based on the rectangular and the two-term MSD windows versus SNR. In the three-point algorithms based on the rectangular window only the version 1 is considered. The results provided by the iterative bias-corrected algorithm are also shown in Fig. 3(b). The number of analyzed samples is M = 128, the number of observed cycles is ν = 5.3.

As expected from the theoretical analysis, both versions of the two-point estimators based on the rectangular or the two-term MSD windows and the three-point estimators based on the two-term MSD window provide the same MSE values. Moreover, the three-point estimator based on the rectangular window and the iterative bias-corrected algorithm are almost equal accurate. The best accuracy is ensured by the two-point estimator based on the rectangular window, i.e., by the AM algorithm [8]. Indeed, the related statistical efficiency is very close to 1. Also, the MSE values increase as the number of window term H increases and the worst accuracy is provided by the three-point estimator based on the two-term MSD window, whose statistical efficiency is about 0.27.

3*) Noisy and harmonically distorted complex sinusoid*

When distorted sinusoids are analyzed, the estimated frequency is affected by the interference due to the spectral leakage from harmonics, whose effect decreases as the number of observed signal cycles ν increases. In the considered testing condition, 2nd, 3rd, and 4th harmonics are added to a noisy signal characterized by SNR = 50 dB. The harmonic amplitudes are fixed according to the ratios 4:2:1 and the related Total Harmonic Distortion (THD) is equal to 5%. The MSE values returned by the version 1 of the

two-point and three-point estimators are shown in Fig. 4(a) and Fig. 4(b), respectively as a function of ν. The value of ν is varied in the range [2.51, 12) cycles with a step 1/16 of cycle. For each value of ν, 1000 runs are considered by varying at random the phases of the fundamental and harmonics. It is worth noticing that the version 2 of the algorithms returns almost the same MSE values as the version 1 (only version 1 is used for the three-point estimator based on the rectangular window).

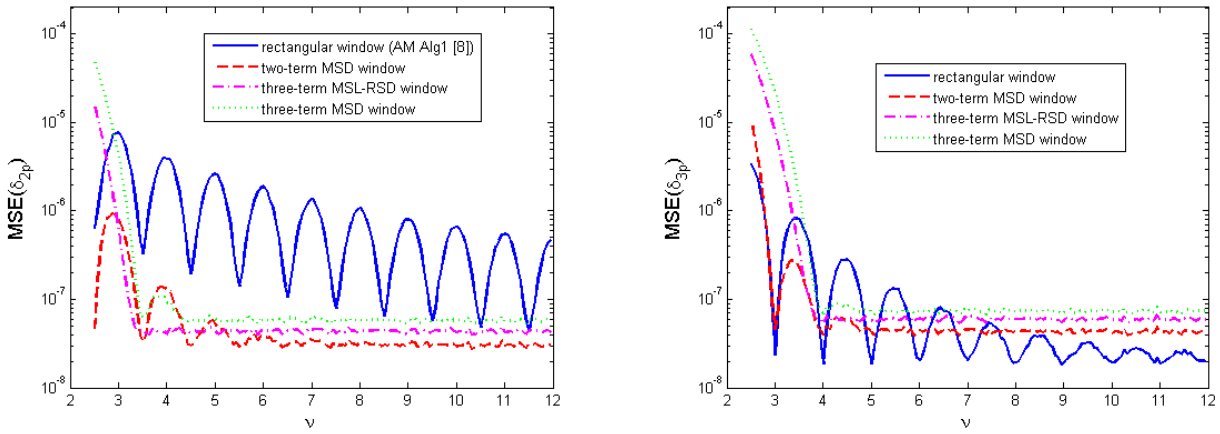

(a) (b)

Fig. 4. MSEs values returned by (a) the MV-IpDTFT(2) and (b) the MV-IpDTFT(3) estimators based on the rectangular, two-term MSD, three-term MSL-RSD, or three-term MSD windows versus the number of observed cycles ν. Noisy and harmonically distorted complex sinusoid with *SNR* = 50 dB and *THD* = 5%. The number of analyzed samples is M = 128.

Fig. 4(a) shows that the best accuracy is achieved when using the two-term MSD window for $\nu < 3$. For $3 < \nu < 5$ the three-term MSL-RSD window outperforms the others in most situations. When $\nu > 5$ the two-term MSD window has to be preferred. Poor accuracy is achieved when the rectangular window is adopted. Conversely, when using a three-point algorithm, the two-term MSD window provides the most accurate estimates for $2 < \nu < 7$, except when δ is close to 0 (quasi-coherent sampling), where the rectangular window allows to achieve the best results. Indeed, in the latter situations the harmonic spectral tones are almost null. For higher value of ν, the contribution of wideband noise on the estimator accuracy prevails on the effect of interference from harmonics and so the rectangular window has to be preferred. Similar behaviors have been obtained for higher THD values.

According to (25), if two-point interpolation is used windowing becomes advantageous when $MSE(\hat{\delta})_{rect(2)}$ is higher than $3.05 \cdot 10^{-8}$, $4.37 \cdot 10^{-8}$, and $5.79 \cdot 10^{-8}$ when the two-term MSD, the three-term MSL-RSD, or the three-term MSD windows are employed, respectively. It is worth noticing that these values are almost equal to those reported in Fig. 4(a) for higher values of ν. Conversely, when three-point interpolation is adopted, windowing allows to achieve more accurate results when $MSE(\hat{\delta})_{rect(3)}$ is higher than $4.34 \cdot 10^{-8}$, $5.97 \cdot 10^{-8}$, and $7.38 \cdot 10^{-8}$ if the two-term MSD, the three-term MSL-RSD, or the three-term MSD windows are employed, respectively. Also these values are very close to those reported in Fig. 4(b) for higher values of ν.

5. Conclusions

In this paper two frequency estimation algorithms proposed in the literature [4], [8] for complex sinusoids have been generalized. The acquired signal is weighted by a generic cosine window in order to ensure high estimation accuracy in the case of signals affected by disturbance tones. The proposed algorithms are based on two interpolation points (MV-IpDTFT(2)) or three interpolation points (MV-IpDTFT(3)). Two different versions have been proposed for each algorithm, based on either DTFT complex values or modules, respectively. All the proposed estimators adopt an iterative procedure in order to minimize the estimation variance due to wideband noise. The expressions of both the proposed estimators and their variances have been derived and verified by means of computer simulation. Computer simulations showed that the AM algorithm [8] provides the most accurate estimate when complex noisy sinusoids are considered. Conversely, in the case of complex harmonically distorted sinusoids, when a relatively small number of signal cycles is observed and the effect of spectral interference from disturbance tones prevails over the influence of wideband noise, then windowing can be required to ensure estimation accuracy. In particular, the constraints under which windowing allows to achieve more accurate estimates have been derived. Also, the proposed procedures can be advantageous when real sinusoids are analyzed due to the detrimental contribution on the estimation accuracy of the spectral interference from

the signal image components. The proposed frequency estimators can be advantageously used in practice when the interference from disturbance tones or narrow-band components dominates the effect of wideband noise and the number of analyzed samples is high enough. Conversely, when the number of analyzed samples is quite small the procedure proposed in [10] provides more accurate frequency estimates.

ACKNOWLEDGMENT

The authors wish to thank the anonymous Reviewers for their helpful comments, which significantly improved the quality of the paper.

APPENDIX A

Proof of Theorem 1

By truncating to the first order term the Taylor's series expansion around δ = -0.5 and δ = 0.5 of the functions $\tilde{W}(-\delta-0.5)$ and $\tilde{W}(-\delta+0.5)$, and reminding that $\tilde{W}(\cdot)$ and $\tilde{W}'(\cdot)$ are even and odd functions, respectively, we obtain:

$$\tilde{W}(-\delta-0.5) \cong \tilde{W}(0.5) + \tilde{W}'(0.5)\delta, \tag{A.1}$$

$$\tilde{W}(-\delta+0.5) \cong \tilde{W}(0.5) - \tilde{W}'(0.5)\delta. \tag{A.2}$$

Using (7) and (8), after some calculations we have:

$$\tilde{W}(0.5) \cong \frac{M}{2\pi}\sum_{h=0}^{H-1}(-1)^h \frac{4a_h}{1-4h^2}, \tag{A.3}$$

and

$$\tilde{W}'(0.5) \cong -\frac{M}{\pi}\sum_{h=0}^{H-1}(-1)^h 4a_h \frac{1+4h^2}{\left(1-4h^2\right)^2}. \tag{A.4}$$

Using (5), (6), (A.1), and (A.2) we achieve:

$$\mathrm{Re}\left\{\frac{X_w(l+0.5)+X_w(l-0.5)}{X_w(l+0.5)-X_w(l-0.5)}\right\}\cong\frac{\tilde{W}(-\delta+0.5)-\tilde{W}(-\delta-0.5)}{\tilde{W}(-\delta+0.5)+\tilde{W}(-\delta-0.5)}\cong-\frac{\tilde{W}'(0.5)}{\tilde{W}(0.5)}\delta. \tag{A.5}$$

By replacing (A.3) and (A.4) in (A.5) the estimator (10) is then achieved.

Similarly, from (5) and (6) it follows that:

$$|X_w(l-0.5)|\cong|A|\tilde{W}(-\delta-0.5), \tag{A.6}$$

$$|X_w(l+0.5)|\cong|A|\tilde{W}(-\delta+0.5). \tag{A.7}$$

Using (A.6) and (A.7), and the expressions (A.1) and (A.2) we have:

$$\frac{|X_w(l+0.5)|-|X_w(l-0.5)|}{|X_w(l-0.5)|+|X_w(l+0.5)|}\cong\frac{\tilde{W}(-\delta+0.5)-\tilde{W}(-\delta-0.5)}{\tilde{W}(-\delta+0.5)+\tilde{W}(-\delta-0.5)}\cong-\frac{\tilde{W}'(0.5)}{\tilde{W}(0.5)}\delta. \tag{A.8}$$

By replacing (A.3) and (A.4) in (A.8) the estimator (11) is finally achieved.

APPENDIX B

Proof of Theorem 2

By truncating to the first order term the Taylor's series expansion around δ = -1, δ = 0, and δ = 1 of the functions $\tilde{W}(-\delta-1)$, $\tilde{W}(-\delta)$, and $\tilde{W}(-\delta+1)$, respectively, and reminding that $\tilde{W}(\cdot)$ and $\tilde{W}'(\cdot)$ are even and odd functions, respectively, we obtain:

$$\tilde{W}(-\delta-1)\cong\tilde{W}(1)+\tilde{W}'(1)\delta, \tag{B.1}$$

$$\tilde{W}(-\delta)\cong\tilde{W}(0)-\tilde{W}'(0)\delta, \tag{B.2}$$

$$\tilde{W}(-\delta+1)\cong\tilde{W}(1)-\tilde{W}'(1)\delta. \tag{B.3}$$

Using (B.1) - (B.3) we have:

$$\tilde{W}(-\delta-1)-\tilde{W}(-\delta+1)\cong2\tilde{W}'(1)\delta, \tag{B.4}$$

and

$$\tilde{W}(-\delta-1)+2\tilde{W}(-\delta)+\tilde{W}(-\delta+1)\cong2\tilde{W}(0)+2\tilde{W}(1)-2\tilde{W}'(0)\delta. \tag{B.5}$$

Expressions (7) and (8) return:

$$\tilde{W}(0) = Ma_0, \tag{B.6}$$

$$\tilde{W}(1) = \frac{Ma_1}{2}, \tag{B.7}$$

$$\tilde{W}'(0) = 0, \tag{B.8}$$

$$\tilde{W}'(1) = M\left(-a_0 + \frac{a_1}{4} + \sum_{h=2}^{H-1}(-1)^h \frac{a_h}{h^2-1}\right). \tag{B.9}$$

From (5) and (6) and the expressions (B.4) and (B.5) we have:

$$\mathrm{Re}\left\{\frac{X_w(l+1)-X_w(l-1)}{X_w(l-1)-2X_w(l)+X_w(l+1)}\right\} \cong \frac{\tilde{W}(-\delta-1)-\tilde{W}(-\delta+1)}{\tilde{W}(-\delta-1)+2\tilde{W}(-\delta)+\tilde{W}(-\delta+1)} \cong \frac{\tilde{W}'(1)\delta}{\tilde{W}(0)+\tilde{W}(1)-\tilde{W}'(0)\delta}. \tag{B.10}$$

By replacing (B.6) – (B.9) into (B.10) the frequency estimator (12) is obtained.

From (5) and (6) it follows that:

$$|X_w(l-1)| \cong A\tilde{W}(-\delta-1), \tag{B.11}$$

$$|X_w(l)| \cong A\tilde{W}(-\delta), \tag{B.12}$$

$$|X_w(l+1)| \cong A\tilde{W}(-\delta+1). \tag{B.13}$$

Using (B.11)-(B.13) and the expressions (B.4) and (B.5) we have:

$$\frac{|X_w(l+1)|-|X_w(l-1)|}{|X_w(l-1)|+2|X_w(l)|+|X_w(l+1)|} \cong \frac{\tilde{W}(-\delta-1)-\tilde{W}(-\delta+1)}{\tilde{W}(-\delta-1)+2\tilde{W}(-\delta)+\tilde{W}(-\delta+1)} \cong \frac{\tilde{W}'(1)\delta}{\tilde{W}(0)+\tilde{W}(1)-\tilde{W}'(0)\delta}. \tag{B.14}$$

From (B.6) – (B.9) and (B.14) the frequency estimator (13) is then achieved.

APPENDIX C

Proof of Theorem 3

In the following the expressions of the two-point frequency estimator variances $\sigma^2_{\hat{\delta}^{(c)}_{2p}}$ and $\sigma^2_{\hat{\delta}^{(m)}_{2p}}$ are derived.

a) *Expression of the variance of the two-point frequency estimator based on complex DTFT values.*

We denote by α_{2p} the ratio in (10), i.e.,

$$\alpha_{2p} \stackrel{\Delta}{=} \gamma_{2p} \frac{X_w(l+0.5)+X_w(l-0.5)}{X_w(l+0.5)-X_w(l-0.5)}. \tag{C.1}$$

Using (4), (C.1) can be expressed as:

$$\alpha_{2p} = \gamma_{2p} \frac{AW(-\delta+0.5)e^{j\phi}+AW(-\delta-0.5)e^{j\phi}+E_{w(0.5)}+E_{w(-0.5)}}{AW(-\delta+0.5)e^{j\phi}-AW(-\delta-0.5)e^{j\phi}+E_{w(0.5)}-E_{w(-0.5)}}. \tag{C.2}$$

By dividing both numerator and denominator of (C.2) by $AW(-\delta+0.5)e^{j\phi}-AW(-\delta-0.5)e^{j\phi}$ we have:

$$\alpha_{2p} = \gamma_{2p} \frac{\dfrac{\delta}{\gamma_{2p}}+\dfrac{E_{w(0.5)}+E_{w(-0.5)}}{AW(-\delta+0.5)e^{j\phi}-AW(-\delta-0.5)e^{j\phi}}}{1+\dfrac{E_{w(0.5)}-E_{w(-0.5)}}{AW(-\delta+0.5)e^{j\phi}-AW(-\delta-0.5)e^{j\phi}}}. \tag{C.3}$$

Since $\left|AW(-\delta+0.5)e^{j\phi}-AW(-\delta-0.5)e^{j\phi}\right| >> \left|E_{w(0.5)}-E_{w(-0.5)}\right|$ for assumption, from (C.3) it follows:

$$\alpha_{2p} \cong \gamma_{2p}\left\{\frac{\delta}{\gamma_{2p}}+\frac{E_{w(0.5)}+E_{w(-0.5)}}{Ae^{j\phi}[W(-\delta+0.5)-W(-\delta-0.5)]}\right\}\left\{1-\frac{E_{w(0.5)}-E_{w(-0.5)}}{Ae^{j\phi}[W(-\delta+0.5)-W(-\delta-0.5)]}\right\}. \tag{C.4}$$

In the product, the term representing the multiplication of the two terms related to the DTFT of wideband noise is very small (with high probability) as compared with the other terms and it can be neglected. Thus, after some simple calculations (C.4) becomes:

$$\alpha_{2p} \cong \delta + \mathrm{Re}\left\{\frac{(\gamma_{2p}-\delta)E_{w(0.5)}+(\gamma_{2p}+\delta)E_{w(-0.5)}}{Ae^{j\phi}[W(-\delta+0.5)-W(-\delta-0.5)]}\right\}+ j\,\mathrm{Im}\left\{\frac{(\gamma_{2p}-\delta)E_{w(0.5)}+(\gamma_{2p}+\delta)E_{w(-0.5)}}{Ae^{j\phi}[W(-\delta+0.5)-W(-\delta-0.5)]}\right\}. \tag{C.5}$$

Using (10), (C.5) provides:

$$\begin{aligned}\sigma^2_{\hat{\delta}^{(c)}_{2p}} \cong & \frac{(\gamma_{2p}-\delta)^2\,\mathrm{var}\left[\mathrm{Re}\{E_{w(0.5)}\}\right]+(\gamma_{2p}+\delta)^2\,\mathrm{var}\left[\mathrm{Re}\{E_{w(-0.5)}\}\right]}{A^2\left[\tilde{W}(-\delta+0.5)+\tilde{W}(-\delta-0.5)\right]^2} \\ & + \frac{2(\gamma_{2p}^2-\delta^2)\rho\left[\mathrm{Re}\{E_{w(0.5)}\},\mathrm{Re}\{E_{w(-0.5)}\}\right]std\left[\mathrm{Re}\{E_{w(0.5)}\}\right]std\left[\mathrm{Re}\{E_{w(-0.5)}\}\right]}{A^2\left[\tilde{W}(-\delta+0.5)+\tilde{W}(-\delta-0.5)\right]^2},\end{aligned} \tag{C.6}$$

in which:

$$\mathrm{var}\left[\mathrm{Re}\left\{E_{w(0.5)}\right\}\right]=\mathrm{var}\left[\mathrm{Re}\left\{E_{w(-0.5)}\right\}\right]=\sigma_{X_w}^2, \tag{C.7}$$

where $\sigma_{X_w}^2$ is the variance of the DTFT samples [24]:

$$\sigma_{X_w}^2 \cong \frac{M}{2} NNPG\,\sigma^2, \tag{C.8}$$

in which *NNPG* is the window Normalized Noise Power Gain [23] given by [14]:

$$NNPG = a_0^2 + 0.5\sum_{h=1}^{H-1} a_h^2, \tag{C.9}$$

and

$$\rho\left[\mathrm{Re}\left\{E_{w(0.5)}\right\}, \mathrm{Re}\left\{E_{w(-0.5)}\right\}\right]=-\rho_1, \tag{C.10}$$

where ρ_1 is the correlation coefficient between two DTFT spectral samples located one bin apart, which is equal to [24], [25]:

$$\rho_1 = \frac{a_0 a_1 + 0.5\sum_{h=1}^{H-2} a_h a_{h+1}}{NNPG}. \tag{C.11}$$

It is worth noticing that (C.10) assumes negative values since the variables $E_{w(0.5)}$ and $E_{w(-0.5)}$ have opposite signs.

Finally, by replacing (C.7), (C.8), (C.10), and $SNR = A^2/\sigma^2$ into (C.6), the expression (14) follows.

b) *Expression of the variance of the two-point frequency estimator based on DTFT modules.*

By applying the law of uncertainty propagation [26] to (11) and using (5) and (6) we obtain:

$$\begin{aligned}\sigma_{\hat{\delta}_{2p}^{(m)}}^2 \cong & \frac{1}{\left[\tilde{W}(-\delta+0.5)+\tilde{W}(-\delta-0.5)\right]^2} \\ & \times \frac{4\gamma_{2p}^2\left[\tilde{W}^2(-\delta+0.5)+\tilde{W}^2(-\delta-0.5)-2\rho_1\tilde{W}(-\delta+0.5)\tilde{W}(-\delta-0.5)\right]}{A^2\left[\tilde{W}(-\delta+0.5)+\tilde{W}(-\delta-0.5)\right]^2}\sigma_{X_w}^2.\end{aligned} \tag{C.12}$$

From (A.5) with $\gamma_{2p} = -\tilde{W}(-0.5)/\tilde{W}'(-0.5)$ we achieve $\tilde{W}(-\delta-0.5) \cong \tilde{W}(-\delta+0.5)(\gamma_{2p}-\delta)/(\gamma_{2p}-\delta)$. By replacing that expression, (C.8), and $SNR = A^2/\sigma^2$ in the second factor in the right hand side of (C.12) we finally obtain the expression (14).

APPENDIX D

Proof of Theorem 4

In the following the expressions of the three-point frequency estimator variances $\sigma^2_{\hat{\delta}^{(c)}_{3p}}$ and $\sigma^2_{\hat{\delta}^{(m)}_{3p}}$ are derived.

a) *Expression of the variance of the three-point frequency estimator based on complex DTFT values*

We denote by α_{3p} the ratio in (12), i.e.,

$$\alpha_{3p} \stackrel{\Delta}{=} \gamma_{3p} \frac{X_w(l+1) - X_w(l-1)}{X_w(l-1) - 2X_w(l) + X_w(l+1)}. \tag{D.1}$$

Using (4), (D.1) can be expressed as:

$$\alpha_{3p} = \gamma_{3p} \frac{AW(-\delta+1)e^{j\phi} - AW(-\delta-1)e^{j\phi} + E_{w(1)} - E_{w(-1)}}{AW(-\delta-1)e^{j\phi} - 2AW(-\delta)e^{j\phi} + AW(-\delta+1)e^{j\phi} + E_{w(-1)} - 2E_{w(0)} + E_{w(1)}}. \tag{D.2}$$

By dividing both the numerator and the denominator of (D.2) by $AW(-\delta-1)e^{j\phi} - 2AW(-\delta)e^{j\phi} + AW(-\delta+1)e^{j\phi}$ we have:

$$\alpha_{3p} = \gamma_{3p} \frac{\dfrac{\delta}{\gamma_{3p}} + \dfrac{E_{w(1)} - E_{w(-1)}}{AW(-\delta-1)e^{j\phi} - 2AW(-\delta)e^{j\phi} + AW(-\delta+1)e^{j\phi}}}{1 + \dfrac{E_{w(-1)} - 2E_{w(0)} + E_{w(1)}}{AW(-\delta-1)e^{j\phi} - 2AW(-\delta)e^{j\phi} + AW(-\delta+1)e^{j\phi}}}. \tag{D.3}$$

Since $\left|AW(-\delta-1)e^{j\phi} - 2AW(-\delta)e^{j\phi} + AW(-\delta+1)e^{j\phi}\right| >> \left|E_{w(-1)} - 2E_{w(0)} + E_{w(1)}\right|$ for assumption, from (D.3) it follows:

$$\alpha_{3p} \cong \gamma_{3p}\left\{\frac{\delta}{\gamma_{3p}}+\frac{E_{w(1)}-E_{w(-1)}}{Ae^{j\phi}\left[W(-\delta-1)-2W(-\delta)+W(-\delta+1)\right]}\right\} \times\left\{1-\frac{E_{w(-1)}-2E_{w(-1)}+E_{w(-1)}}{Ae^{j\phi}\left[W(-\delta-1)-2W(-\delta)+W(-\delta+1)\right]}\right\}. \tag{D.4}$$

In the product, the term representing the multiplication of the two terms related to the DTFT of wideband noise is very small (with high probability) as compared with the other terms and it can be neglected. Thus, after some simple calculations (D.4) becomes:

$$\alpha_{3p} \cong \delta+\mathrm{Re}\left\{\frac{-(\gamma_{3p}+\delta)E_{w(-1)}+2\delta E_{w(0)}+(\gamma_{3p}-\delta)E_{w(1)}}{Ae^{j\phi}\left[W(-\delta-1)-2W(-\delta)+W(-\delta+1)\right]}\right\} + j\,\mathrm{Im}\left\{\frac{-(\gamma_{3p}+\delta)E_{w(-1)}+2\delta E_{w(0)}+(\gamma_{3p}-\delta)E_{w(1)}}{Ae^{j\phi}\left[W(-\delta-1)-2W(-\delta)+W(-\delta+1)\right]}\right\}. \tag{D.5}$$

Using (12) the expression (D.5) provides:

$$\begin{aligned}\sigma^2_{\hat{\delta}^{(c)}_{3p}} \cong & \frac{(\gamma_{3p}+\delta)^2\,\mathrm{var}\left[\mathrm{Re}\left\{E_{w(-1)}\right\}\right]+4\delta^2\,\mathrm{var}\left[\mathrm{Re}\left\{E_{w(0)}\right\}\right]+(\gamma_{3p}-\delta)^2\,\mathrm{var}\left[\mathrm{Re}\left\{E_{w(1)}\right\}\right]}{A^2\left[\tilde{W}(-\delta-1)+2\tilde{W}(-\delta)+\tilde{W}(-\delta+1)\right]^2} \\ & -\frac{4\delta(\gamma_{3p}+\delta)\rho\left[\mathrm{Re}\left\{E_{w(-1)}\right\},\mathrm{Re}\left\{E_{w(0)}\right\}\right]std\left[\mathrm{Re}\left\{E_{w(-1)}\right\}\right]std\left[\mathrm{Re}\left\{E_{w(0)}\right\}\right]}{A^2\left[\tilde{W}(-\delta-1)+2\tilde{W}(-\delta)+\tilde{W}(-\delta+1)\right]^2} \\ & +\frac{4\delta(\gamma_{3p}-\delta)\rho\left[\mathrm{Re}\left\{E_{w(0)}\right\},\mathrm{Re}\left\{E_{w(1)}\right\}\right]std\left[\mathrm{Re}\left\{E_{w(0)}\right\}\right]std\left[\mathrm{Re}\left\{E_{w(1)}\right\}\right]}{A^2\left[\tilde{W}(-\delta-1)+2\tilde{W}(-\delta)+\tilde{W}(-\delta+1)\right]^2} \\ & -\frac{2(\gamma^2_{3p}-\delta^2)\rho\left[\mathrm{Re}\left\{E_{w(-1)}\right\},\mathrm{Re}\left\{E_{w(1)}\right\}\right]std\left[\mathrm{Re}\left\{E_{w(-1)}\right\}\right]std\left[\mathrm{Re}\left\{E_{w(1)}\right\}\right]}{A^2\left[\tilde{W}(-\delta-1)+2\tilde{W}(-\delta)+\tilde{W}(-\delta+1)\right]^2},\end{aligned} \tag{D.6}$$

in which:

$$\mathrm{var}\left[\mathrm{Re}\left\{E_{w(-1)}\right\}\right]=\mathrm{var}\left[\mathrm{Re}\left\{E_{w(0)}\right\}\right]=\mathrm{var}\left[\mathrm{Re}\left\{E_{w(-1)}\right\}\right]=\sigma^2_{X_w}, \tag{D.7}$$

where $\sigma^2_{X_w}$ is the variance of the DTFT samples, given by (C.8),

$$\rho\left[\mathrm{Re}\left\{E_{w(-1)}\right\},\mathrm{Re}\left\{E_{w(0)}\right\}\right]=\rho\left[\mathrm{Re}\left\{E_{w(0)}\right\},\mathrm{Re}\left\{E_{w(1)}\right\}\right]=-\rho_1, \tag{D.8}$$

in which ρ_1 is the correlation coefficient between two DTFT spectral samples located a bin apart, whose expression is given in (C.11), and

$$\rho\left[\mathrm{Re}\left\{E_{w(-1)}\right\},\mathrm{Re}\left\{E_{w(1)}\right\}\right]=\rho_2, \tag{D.9}$$

where ρ_2 is the correlation coefficient between two DTFT spectral samples located two bins apart, which is equal to [24], [25]:

$$\rho_2 = \frac{a_0 a_2 + 0.25 a_1^2 + 0.5 \sum_{h=1}^{H-3} a_h a_{h+2}}{NNPG}. \tag{D.10}$$

Finally, by replacing (D.7), (C.8), (D.8), and (D.9) into (D.6), and remembering that $SNR = A^2 / \sigma^2$, the expression (20) follows.

b) *Expression of the variance of the three-point frequency estimator based on DTFT modules*

For the sake of simplicity, the following notation is adopted:

$$|X_w(l-1)| \stackrel{\Delta}{=} u_1,\ |X_w(l)| \stackrel{\Delta}{=} u_2,\ |X_w(l+1)| \stackrel{\Delta}{=} u_3. \tag{D.11}$$

From (5) we have:

$$u_1 \cong A\tilde{W}(-\delta - 1),\ u_2 \cong A\tilde{W}(-\delta), u_3 \cong A\tilde{W}(-\delta + 1). \tag{D.12}$$

By applying the law of uncertainty propagation [26] to (13) we obtain:

$$\sigma^2_{\hat{\delta}^{(m)}_{3p}} = \left[\left(\frac{\partial \hat{\delta}^{(m)}_{3p}}{\partial u_1} \right)^2 + \left(\frac{\partial \hat{\delta}^{(m)}_{3p}}{\partial u_2} \right)^2 + \left(\frac{\partial \hat{\delta}^{(m)}_{3p}}{\partial u_3} \right)^2 + 2 \frac{\partial \hat{\delta}^{(m)}_{3p}}{\partial u_1} \frac{\partial \hat{\delta}^{(m)}_{3p}}{\partial u_2} \rho_1 \right. \tag{D.13}$$
$$\left. + 2 \frac{\partial \hat{\delta}^{(m)}_{3p}}{\partial u_2} \frac{\partial \hat{\delta}^{(m)}_{3p}}{\partial u_3} \rho_1 + 2 \frac{\partial \hat{\delta}^{(m)}_{3p}}{\partial u_1} \frac{\partial \hat{\delta}^{(m)}_{3p}}{\partial u_3} \rho_2 \right] \sigma^2_{X_w},$$

where $\sigma^2_{X_w}$, ρ_1, and ρ_2 are given by (C.8), (C.11), and (D.10), respectively, and

$$\frac{\partial \hat{\delta}^{(m)}_{3p}}{\partial u_1} = -2\gamma_{3p} \frac{u_2 + u_3}{(u_1 + 2u_2 + u_3)^2},\quad \frac{\partial \hat{\delta}^{(m)}_{3p}}{\partial u_2} = -2\gamma_{3p} \frac{u_3 - u_1}{(u_1 + 2u_2 + u_3)^2},\quad \frac{\partial \hat{\delta}^{(m)}_{3p}}{\partial u_3} = 2\gamma_{3p} \frac{u_1 + u_2}{(u_1 + 2u_2 + u_3)^2}.$$

Using (B.11) - (B.14) with $\gamma_{3p} = [\tilde{W}(0) + \tilde{W}(1)] / \tilde{W}'(1)$ we obtain:

$$\frac{\partial \hat{\delta}^{(m)}_{3p}}{\partial u_1} \cong \frac{\delta - \gamma_{3p}}{\tilde{W}(-\delta - 1) + 2\tilde{W}(-\delta) + \tilde{W}(-\delta + 1)},\quad \frac{\partial \hat{\delta}^{(m)}_{3p}}{\partial u_2} \cong \frac{2\delta}{\tilde{W}(-\delta - 1) + 2\tilde{W}(-\delta) + \tilde{W}(-\delta + 1)},$$

and

$$\frac{\partial \hat{\delta}_{3p}^{(m)}}{\partial u_3} \cong \frac{\delta + \gamma_{3p}}{\widetilde{W}(-\delta - 1) + 2\widetilde{W}(-\delta) + \widetilde{W}(-\delta + 1)}.$$

By replacing these expressions, (C.8) and $SNR = A^2 / \sigma^2$ in (D.13), after some simple calculations we finally obtain the expression (20) for the three-point frequency estimator based on DTFT modules.

REFERENCES

[1] D.C. Rife, G.A. Vincent, Use of the discrete Fourier transform in the measurement of frequencies and levels of tones, Bell Syst. Tech. J. 49 (1970) 197-228.

[2] B.G. Quinn, Estimating frequency by interpolation using Fourier coefficients, IEEE Trans. Signal Process. 42 (1994) 1264-1268.

[3] B.G. Quinn, Estimation of frequency, amplitude, and phase from the DFT of a time series, IEEE Trans. Signal Process. 45 (1997) 814-817.

[4] E. Jacobsen, P. Kootsookos, Fast, accurate frequency estimators, IEEE Signal Process. Mag. 24 (2007). 123-125.

[5] C. Candan, A method for fine resolution frequency estimation from three DFT samples, IEEE Signal Process. Lett. 18 (6) (2011) 351-354.

[6] C. Candan, Analysis and further improvement of fine resolution frequency estimation method from three DFT samples, IEEE Signal Process. Lett. 20 (9) (2013) 913-916.

[7] Y. Liu, Z. Nie, Z. Zhao, Q.H. Liu, Generalization of iterative Fourier interpolation algorithm for single frequency estimation, Digital Signal Process. 21 (1) (2011) 141-149.

[8] E. Aboutanios, B. Mulgrew, Iterative frequency estimation by interpolation on Fourier coefficients, IEEE Trans. Signal Process. 53(4) (2005) 1237-1241.

[9] J-R Liao, S. Lo, Analytical solutions for frequency estimators by interpolation of DFT coefficients, Signal Process. 100 (2014) 93-100.

[10] C. Candan, Fine resolution frequency estimation from three DFT samples: case of windowed data, Signal Process. 114 (2015) 245-250.

[11] U. Orguner, C. Candan, A fine-resolution frequency estimator using an arbitrary number of DFT coefficients, Signal Process. 105 (2014) 17-21.

[12] J. Schoukens, R. Pintelon, H. Van Hamme, The interpolated fast Fourier transform: a comparative study, IEEE Trans. Instrum. Meas. vol. 41 (2) (1992) 226-232.

[13] C. Offelli, D. Petri, The influence of windowing on the accuracy of multifrequency signal parameter estimation, IEEE Trans. Instrum. Meas. 41 (2) (1992) 256-261.

[14] D. Belega, D. Dallet, Multifrequency signal analysis by interpolated DFT method with maximum sidelobe decay windows, Measurement 42 (3) (2009) 420-426.

[15] D. Belega, D. Dallet, D. Petri, Statistical description of the sine-wave frequency estimator provided by the interpolated DFT method, Measurement 45 (1) (2012) 109-117.

[16] K. Duda, DTFT interpolation algorithm for Kaiser-Bessel and Dolph-Chebyshev windows, IEEE Trans. Instrum. Meas. 60 (3) (2011) 784-790.

[17] D. Agrež, Weighted multipont interpolated DFT to improve amplitude estimation of multifrequency signal. IEEE Trans. Instrum. Meas. 51(2) (2002) 287-292.

[18] D. Belega, D. Dallet, High-accuracy frequency estimation via weighted multipoint interpolated DFT, IET Sci., Meas. Technol. 2(1) (2008) 1-8.

[19] D. Belega, D. Dallet, D. Petri, Accuracy of sine-wave frequency estimation by multipoint interpolated DFT approach, IEEE Trans. Instrum. Meas. 59 (11) (2010) 2808-2815.

[20] D. Belega, D. Petri, D. Dallet, Frequency estimation of a sinusoidal signal via a three-point interpolated DFT method with high image component interference rejection capability, Digital Signal Process. 24 (1) (2014) 162-169.

[21] A.H. Nuttall, Some windows with very good sidelobe behavior, IEEE Trans. Acoust., Speech, Signal Proces. 29 (1) (1981) 84–91.

[22] A. Ferrero, R. Ottoboni, High-accuracy Fourier analysis based on synchronous sampling techniques, IEEE IEEE Trans. Instrum. Meas. 41 (6) (1992) 780-785.

[23] F.J. Harris, On the use of windows for harmonic analysis with the discrete Fourier transform, Proc. of the IEEE 66 (1) (1978) 51–83.

[24] M. Novotný, D. Slepička, M. Sedláček, Uncertainty analysis of the RMS value and phase in frequency domain by noncoherent sampling, IEEE Trans. Instrum. Meas. 56 (3) (2007) 983-989.

[25] C. Offeli, D. Petri D, Weighting effect on the discrete time Fourier transform of noisy signals, IEEE Trans. Instrum. Meas. 40 (6) (1991) 972-978.

[26] Guide for the expression of Uncertainty in Measurements, International Organization for Standardization, Switzerland, 1993.